

An Inside Look at the Ti-MoS₂ Contact in Ultra-thin Field Effect Transistor with Atomic Resolution

Ryan J. Wu¹⁺, Sagar Udyavara¹⁺, Rui Ma², Yan Wang³, Manish Chhowalla³, Steven J. Koester²,

Matthew Neurock^{1*}, K. Andre Mkhoyan^{1*}

¹Department of Chemical Engineering and Material Science, University of Minnesota, Minneapolis, MN 55455

²Department of Electrical and Computer Engineering, University of Minnesota, Minneapolis, MN 55455

³Department of Material Science and Engineering, Rutgers University, Piscataway, NJ 08854

⁺ These authors contributed equally to this work

^{*}Corresponding authors. E-mail: mneurock@umn.edu (MN) and mkhoyan@umn.edu (KAM)

Abstract: Two-dimensional molybdenum disulfide (MoS₂) is an excellent channel material for ultra-thin field effect transistors. However, high contact resistance across the metal-MoS₂ interface continues to limit its widespread realization. Here, using atomic-resolution analytical scanning transmission electron microscopy (STEM) together with first principle calculations, we show that this contact problem is a fundamental limitation from the bonding and interactions at the metal-MoS₂ interface that cannot be solved by improved deposition engineering. STEM analysis in conjunction with theory shows that when MoS₂ is in contact with Ti, a metal with a high affinity to form strong bonds with sulfur, there is a release of S from Mo along with the formation of small Ti/Ti_xS_y clusters. A destruction of the MoS₂ layers and penetration of metal can also be expected. The design of true high-mobility metal-MoS₂ contacts will require the optimal selection of the metal or alloy based on their bonding interactions with the MoS₂ surface. This can be advanced by evaluation of binding energies with increasing the number of atoms within metal clusters.

Transition metal dichalcogenides (TMDs), with the chemical formula MX_2 , where M is a group IV, V, or VI transition metal and X is the chalcogenide, make up a sub-group of materials with highly tunable electronic properties within the family of van der Waals (vdW) bonded two-dimensional (2D) materials. Ultra-thin field effect transistors (FETs) using molybdenum disulfide (MoS_2) as the channel material have shown excellent performance, making them viable for sub-10 nm node devices (1-5). However, optimizing the contact between the 2D semiconductor and the 3D metal electrode with direct chemical bonding remains a challenge due to the high contact resistance (6-9) commonly attributed to Fermi level pinning at the metal- MoS_2 interface (10-12). Experimental and computational reports have shown or suggested that surface states created from adsorbed contaminants and damage by kinetic energy transfer from metal deposition can pin the Fermi level and increase the contact resistance (13, 14). Therefore, it is largely believed that continued improvement of the metal deposition and FET fabrication will lead to “clean” metal-TMD interfaces without pinning (11, 15, 16). However, whether this challenge is one in optimizing the deposition of the metal on MoS_2 or, instead, due to the fundamental bonding and chemistry at metal- MoS_2 interface is still unknown. While it is possible to engineer metal- MoS_2 contact with vdW interactions either by incorporating an intermediate layer (17, 18), by transferring an entire metal film (5), or by using a metal with very low affinity to bond with sulfur, the transmittance of charge carriers will be limited by the vdW barrier. Ultimately, moderate interatomic bonding that anchors the metal to the MoS_2 without restructuring the metal- MoS_2 interface is needed for true high-mobility charge transfer in MoS_2 embedded FETs.

Here, using atomic-resolution analytical scanning transmission electron microscopy (STEM), we directly image and characterize a contamination-free, deposition damage-free interface between Ti metal electrode and an MoS_2 channel in a FET to address the issue of pinning. Ti possesses a very strong affinity for sulfur with a Ti-S bond dissociation energy of -3.69 eV (vs. that of Mo-S at -2.35 eV) (19). Consequentially, it is often used as the metal electrode as it provides a strong contact with the MoS_2 surface which is desirable for effective charge injection into the MoS_2 (20-22). Annular dark-field (ADF)-STEM imaging is used in conjunction with electron energy-loss spectroscopy (EELS) to measure the changes in

the atomic structure as well as the electronic structure at each layer of MoS₂. First principle density functional theory (DFT) calculations are carried out to understand these observed changes in atomic and electronic structure of the Ti-MoS₂ contact and to help identify possible paths to improve metal-MoS₂ interface performance.

Figure 1(a) shows the schematic layout of the FETs studied here, where the Ti layer from the metal contact directly interfaces with the MoS₂ channel. A low-magnification cross-sectional ADF-STEM image of such a FET is shown in Figure 1(b) where the Au/Ti contact and Si/SiO₂ substrate bookend the layers of the device. Only some of the individual layers are visible at this magnification. A higher-magnification image of the FET, where the metal contact, MoS₂ channel, and all other structural layers are visible, is provided in the SI (see Figure S1). EELS spectra of the oxygen K edge measured from the Ti-MoS₂ interfacial layers show a negligible oxygen content (see Figure S2 in SI), which rules out possible water or oxide contaminants (15) at the Ti-MoS₂ interface during Ti deposition. Under the low-energy conditions of electron beam evaporation-dependent physical vapor deposition, as discussed in the Methods section of the SI, no physical damage to MoS₂ layers should be occurring due to the Ti deposition.

Figure 1(c) shows a high-magnification ADF-STEM image of the Ti-MoS₂ interface, where the individual MoS₂ layers can be clearly identified. As can be seen at this magnification, the Ti layer forms a non-uniform interface with the MoS₂. Along the Ti-MoS₂ interface, there are clear identifiable areas where the Ti extends into the MoS₂ channel and visibly alters the structure of the topmost layer. Next to them are areas where the Ti retreats and small void pockets are formed, leaving the topmost MoS₂ layer pristine. This non-uniformity suggest that the Ti atoms tend to cluster on MoS₂ during deposition, a behavior suggested or predicted before (16) but never directly observed experimentally (see Figure S3 in SI for additional images).

The atomic-resolution ADF-STEM image in Figure 1(d) obtained from one of these Ti-clustered areas shows that the topmost MoS₂ layer is indeed completely degraded and barely identifiable. It also

shows that the intensity of the ADF signal in the Ti region directly above the 1st MoS₂ layer is lower and gradually increases with distance away from the MoS₂. This suggests that the Ti is less dense directly above the MoS₂, an observation with two possible explanations: (i) the presence of more void pockets along the electron beam direction, which is likely, or (ii) the presence of a Ti sublayer with lower atomic density. The viability of the second possibility will be considered later. These observations combined with earlier predictions suggest that the non-uniformity of the Ti-MoS₂ interface may be the result of chemical bonding between Ti and S that drives a restructuring of the Ti-MoS₂ interface to form more energetically-favored structures and, as such, would be intrinsic to the Ti contact.

To measure the changes to the electronic structure of MoS₂ caused by the Ti contact, layer-by-layer EELS analysis was performed across the Ti-MoS₂ interface. Electronic excitations from the sulfur core *2p* states to the empty states of conduction band are recorded from each MoS₂ layer using core-level EELS. These experiments measure changes in the local electronic density of states (DOS) of the conduction band, which are sensitive to the local bonding environment of the probed atoms (23). An example of such a core-level EELS dataset is presented in the SI (Figure S4). Figure 2(a) shows two S L₂₃ core-level EELS edges measured from the MoS₂ channel: one from layer 1, the topmost MoS₂ layer directly in contact with Ti, and the other from layer 5, which is far away from the interface and represents the bulk-like MoS₂ layer. The dominating features of the S L₂₃ edge fine structure, peaks I and II, composed of S 3*s* and 3*d* partial-DOS (24) are quantifiably different in these measured spectra, as can be seen in the difference spectrum shown in Figure 2(a). In comparison, these peaks are more subdued in layer 1 - a strong indication that the atomic structure of this layer has lost its periodicity considerably (23), which is consistent with observations from the ADF-STEM images. Similar EELS analysis on an area of MoS₂ not in contact with Ti shows no differences between the first and fifth MoS₂ layers, as can be seen in Figure S5 in the SI. Thus, only areas of the MoS₂ channel directly in contact with Ti show changes in their electronic band structure.

Although the atomic-resolution ADF-STEM images of the interface show clear structural degradations in the first layer, changes in the electronic structure can potentially propagate to deeper layers.

Figure 2(b) shows a set of core-level EELS measurements from each of the first seven MoS₂ layers and at one additional position in the Ti contact directly above the MoS₂. Changes in the prominence of peaks I and II of the S L₂₃ edge were systematically quantified for all the layers (25). The fraction of the spectrum at each layer with interfacial character (reference layer 1) is plotted in Figure 2(c). The results show layer 2 and even layer 3 possess considerable interfacial character in their S L₂₃ edge. These measurements show the effects of the Ti contact on the MoS₂ channel go beyond the surface layer and, consequently, the pinning of the Fermi level likely extends deeper into the layers of MoS₂ and is not limited only to the interface as previously speculated (10, 11). The effects of STEM probe broadening in the analysis of these results are inconsequential, as the evaluated beam broadening for these experiments was less than 5.5 Å (or less than a MoS₂ layer) and affects in quadrature.

Since the crystal structure of the topmost layer of MoS₂ is degraded in areas in contact with Ti, the presence of Ti atoms in deeper MoS₂ layers cannot be ruled out. Core-level EELS of the Ti L₂₃ edge was measured across the first seven MoS₂ layers. An example of EELS Ti L₂₃ edge dataset can be found in the SI (Figure S4). Figure 2(d) shows the integrated intensity of the Ti L₂₃ edge at each layer using the spectrum from layer 0, which is the position directly above the MoS₂, as a reference. Surprisingly, in addition to layer 1, layers 2 and 3 also show an appreciable amount of Ti present. The amount of Ti in layers 2 and 3 is significant enough to affect the electronic structure of MoS₂ and explain the observed changes in the fine structure of the S L₂₃ edge. However, they are not high enough to affect the pristine-like view of the atomic structure as imaged in projection using ADF-STEM. The penetration of Ti into MoS₂ can result in reduction of the density of atoms in the Ti sublayer just above the interface, which, as alluded earlier, may be the cause of the reduced contrast observed in ADF-STEM images (Figure 1(d)).

DFT calculations were carried out to determine the structure, bonding and interactions of Ti atoms with MoS₂ layers. These simulations examined the systematic addition of individual Ti atoms onto the surface of a monolayer of MoS₂ in order to mimic the experimental deposition (see methods and SI for procedure). This “single-atom-addition” approach, while computationally demanding, provides more

insight into atomic processes occurring at the metal-MoS₂ interface as compared to the addition of whole layers of Ti in a “metal-MoS₂-slab” approach (20-22, 26).

Figure 3(a) shows the simulated lowest energy structures of the Ti-MoS₂ interfaces after the addition one, two, three and five Ti atoms to the top of a MoS₂ surface. While many more Ti atoms are involved at the actual metal contact with MoS₂, these smaller model systems can provide sufficient insight as to what may be occurring during Ti deposition. The simulations show that the strong interactions between the Ti and S disrupt the MoS₂ interface by pulling S atoms out of the MoS₂ surface when two or more Ti atoms are present to form a titanium sulfide cluster. These Ti_xS_y clusters are highly stable structures due to the strong Ti-S bond energies. While such interactions lead to a stable Ti-MoS₂ configuration, they also destroy the pristine crystal structure of MoS₂. This not only disrupts the periodic structure of pure MoS₂ but also introduces significant non-periodicity in the Ti clusters above the MoS₂ layer. Furthermore, it appears that relatively large openings in the MoS₂ layer can also form near the site of the lattice disruption (Figure 3(b)). These “nanopores” in the MoS₂ can be large enough to allow Ti atoms to penetrate into deeper layers, which would explain the presence of appreciable amount of Ti in the 2nd and 3rd layers of MoS₂ observed in the EELS measurements. It is worth noting that these simulations were performed without the effects of temperature, which can further enhance destructiveness of the Ti-MoS₂ bonds. Ti atoms were added to the system without kinetic energy to intentionally avoid engineering aspects of metal contact deposition. The simulation results demonstrate that the disruption of the MoS₂ lattice from the Ti contact is due to the inherent bonding and chemistry of the Ti-MoS₂ system and not a result of kinetic energy transfer during deposition as was speculated in literature (11, 27).

These DFT calculations also provide a direct comparison between the electronic structures and DOS of a pristine monolayer of MoS₂ and that of a five Ti atom-MoS₂ interfacial system (Figure 3(c)). Not surprisingly, the Ti interactions with MoS₂ significantly alters the electronic structure of MoS₂ because of the bonded Ti atoms and loss of symmetry. The total as well as S 3s+3d partial DOS of the Ti distorted-MoS₂ show a dramatic reduction and broadening of sharp features compared to those of the pristine MoS₂,

which is consistent with the broadening of peaks I and II in the S L_{23} edge fine structure observed earlier (Figure 2(a)).

The DFT calculations of the metal-MoS₂ interface, using the same “single-atom-addition” approach, were extended to metals with significantly weaker metal-sulfur bonds by using Au and In. Both of these metals have significantly lower Gibbs free energies for metal-sulfide formation than Mo or Ti and, therefore, are expected to form very weak bonds with S, which limits the restructuring of the metal-MoS₂ interface (28). The simulated structures for five Au atom-MoS₂ interfaces and five In atom-MoS₂ interfaces (Figure 3(d)) show that Au as well as In weakly bind to the MoS₂ via weak vdW interactions, which leaves the structure of the MoS₂ surface almost unaltered. At first glance, this may appear to be a major advantage having a metal-MoS₂ interface with minimum or non-existent Fermi level pinning. However, in this case, the vdW gap acts a tunnel barrier that limits charge transport, which is a fundamental limitation of another kind.

Examining the binding energies of single metal atoms onto the MoS₂ surface provides initial insights into metal-sulfur cluster formation and propensity for disruption of the MoS₂ surface. The calculations of these binding energies as well as the metal cluster binding energies on MoS₂ presented above may provide a way to more rapidly screen and design different metals as well as metal alloys as contact materials with MoS₂ that avoid pinning and vdW gaps. Calculated binding energies for a single metal atom on MoS₂ for a wide range of different metals are presented in SI (Table S1). Even with just a single-atom, systematic patterns begin to show the similarity of weak binding for In and Au compared to the destructiveness of Ti on MoS₂, which is consistent with experimental results. The simulations suggest that metals or metal alloys with more moderate binding energies to MoS₂ (those that lie between In (-1.49 eV) and Ti (-3.09 eV)) may be optimal as they would provide a strong enough contact with the MoS₂ surface to enable charge injection yet avoid strong covalent bonds that lead to a disruption of the metal-MoS₂ interface.

In conclusion, atomic-resolution characterization of a the Ti-MoS₂ interface in a FET using ADF-STEM imaging and layer-by-layer EELS shows that the commonly believed premise that improved metal deposition and FET fabrication will solve the pinning problem at the metal-MoS₂ interface will need to be reconsidered. Fermi level pinning is likely unavoidable when a metal with high affinity to form strong bonds with sulfur such as Ti is used regardless of deposition engineering. A metal or engineered metallic alloy with just the right affinity to form a moderate chemical bond with sulfur may be a solution to avoid pinning. A simpler way to evaluate the suitability of a metal or an alloy as a contact material with MoS₂ that has a potential to avoid pinning or forming van-der-Waals gap, is by calculating the binding energies and atomic structures of a-few-atom big metallic clusters that are brought together on the surface of MoS₂.

Acknowledgements: STEM analysis was performed in the Characterization Facility of the University of Minnesota, which receives partial support from the NSF through the MRSEC program. We also thank the Minnesota Supercomputing Institute at the University of Minnesota for computational support. This project was partially supported by the MRSEC program of the National Science Foundation under Award DMR-1420013, the C-SPIN, one of the six SRC STARnet Centers, sponsored by MARCO and DARPA and DTRA through Grant No. HDTRA 1-14-1-0042. R.J.W and K.A.M. conceived the study and wrote the paper with assistance and input from S.U., M.N., M.C and Y.W.

Contributions: R.J.W. and K.A.M. conceived the study and wrote the paper with assistance and input from S.U., M.N., M.C. and Y.W. R.J.W. conducted STEM experiments and processed the results with guidance from K.A.M. S.U. performed all DFT simulations with guidance from M.N. Ti-MoS₂ devices were fabricated by R.M. with guidance from S.J.K.

References and Notes:

1. B. Radisavljevic, A. Radenovic, J. Brivio, J. Giacometti, A. V. Kis, Single-layer MoS₂ transistors. *Nature Nanotechnology* **6**, 147-150 (2011).
2. J. Shim, H.-Y. Park, D.-H. Kanh, J.-O. Kim, S.-H. Jo, Y. Park, J.H. Park, Electronic and optoelectronic devices based on two-dimensional materials: from fabrication to application. *Advanced Electronic Materials* **3**, 1600364 (2017).
3. M. Chhowalla, D. Jena, H. Zhang, Two-dimensional semiconductors for transistors. *Nature Reviews Materials* **1**, 16052 (2016).
4. S. Das, H.-Y. Chen, A. V. Penumatcha, J. Appenzeller, High performance multilayer MoS₂ transistors with scandium contacts. *Nano Letters* **13**, 100-105 (2013).
5. Y. Liu, J. Guo, E. Zhu, L. Liao, S.-J. Lee, M. Ding, I. Shakir, V. Gambin, Y. Huang, X. Duan, Approaching the Schottky–Mott limit in van der Waals metal–semiconductor junctions. *Nature* **557**, 696-700 (2018).
6. A. Allain, J. Kang, K. Banerjee, A. Kis, Electrical contacts to two-dimensional semiconductors. *Nature Materials* **14**, 1195-1205 (2015).
7. H. Liu, A. T. Neal, P. D. Ye, Channel length scaling of MoS₂ MOSFETs. *ACS Nano* **6**, 8563-8569 (2012).
8. H. Liu, M. Si, S. Najmaei, A. T. Neal, Y. Du, P. M. Ajayan, J. Lou, P. D. Ye, Statistical study of deep submicron dual-gated field-effect transistors on monolayer chemical vapor deposition molybdenum disulfide films. *Nano Letters* **13**, 2640-2646 (2013).
9. R. Kappera, D. Voiry, S. E. Yalcin, B. Branch, G. Gupta, A. D. Mohite, M. Chhowalla, Phase-engineered low-resistance contacts for ultrathin MoS₂ transistors. *Nature Materials* **13**, 1128-1134 (2014).
10. C. Gong, L. Colombo, R. M. Wallace, K. Cho, The unusual mechanism of partial Fermi level pinning at metal–MoS₂ interfaces. *Nano Letters* **14**, 1714-1720 (2014).
11. C. Kim, I. Moon, D. Lee, M. S. Choi, F. Ahmed, S. Nam, Y. Cho, H.-J. Shin, S. Park, W. J. Yoo, Fermi level pinning at electrical metal contacts of monolayer molybdenum dichalcogenides. *ACS Nano* **11**, 1588-1596 (2017).
12. Y. Du, L. Yang, H. Liu, P. D. Ye, Contact research strategy for emerging molybdenum disulfide and other two-dimensional field-effect transistors. *APL Materials* **2**, 092510 (2014).
13. C. M. Smyth, R. Addou, S. McDonnell, C. L. Hinkle, R. M. Wallace, Contact metal–MoS₂ interfacial reactions and potential implications on MoS₂-based device performance. *The Journal of Physical Chemistry C* **120**, 14719-14729 (2016).
14. S. McDonnell, C. Smyth, C. L. Hinkle, R. M. Wallace, MoS₂-titanium contact interface reactions. *ACS Applied Materials & Interfaces* **8**, 8289-8294 (2016).
15. C. D. English, G. Shine, V. E. Dorgan, K. C. Saraswat, E. Pop, Improved contacts to MoS₂ transistors by ultra-high vacuum metal deposition. *Nano Letters* **16**, 3824-3830 (2016).
16. C. Gong, C. Huang, J. Miller, L. Cheng, Y. Hao, D. Cobden, J. Kim, R. S. Ruoff, R. M. Wallace, K. Cho, X. Xu, Y. J. Chabal, Metal contacts on physical vapor deposited monolayer MoS₂. *ACS Nano* **7**, 11350-11357 (2013).
17. W. S. Leong, X. Luo, Y. Li, K. H. Khoo, S. Y. Quek, J. T. L. Thong, Low resistance metal contacts to MoS₂ devices with nickel-etched-graphene electrodes. *ACS Nano* **9**, 869-877 (2015).
18. J. Wang, Q. Yao, C.-W. Huang, X. Zou, L. Liao, S. Chen, Z. Fan, K. Zhang, W. Wu, X. Xiao, C. Jiang, W.-W. Wu, High mobility MoS₂ transistor with low Schottky barrier contact by using atomic thick h-BN as a tunneling layer. *Advanced Materials* **28**, 8302-8308 (2016).
19. Y.-R. Luo, *Comprehensive Handbook of Chemical Bond Energies*. (CRC Press, Boca Raton, ed. 1, 2007).

20. J. Kang, D. Sarkar, W. Liu, D. Jena, K. Banerjee, A computational study of metal contacts to beyond-graphene 2D semiconductor materials, in *2012 International Electron Devices Meeting*. 17.14.11-17.14.14 (2012).
21. I. Popov, G. Seifert, D. Tománek, Designing electrical contacts to MoS₂ monolayers: a computational study. *Physical Review Letters* **108**, 156802 (2012).
22. J. Kang, W. Liu, D. Sarkar, D. Jena, K. Banerjee, Computational study of metal contacts to monolayer transition-metal dichalcogenide semiconductors. *Physical Review X* **4**, 031005 (2014).
23. R. F. Egerton, *Electron Energy-Loss Spectroscopy in the Electron Microscope*. (Springer, New York, ed. 3, 2011).
24. M. Dadsetani, H. Nejatipour, T. Nouri, First-principles study of the sulfur K and L_{2,3} edges of transition metal disulfide monolayers, MS₂ (M=Mo, W and Re). *Physica E: Low-dimensional Systems and Nanostructures* **73**, 198-206 (2015).
25. D. A. Muller, T. Sorsch, S. Moccio, F. H. Baumann, K. Evans-Lutterodt, G. Timp, The electronic structure at the atomic scale of ultrathin gate oxides. *Nature* **399**, 758-761 (1999).
26. H. Zhong, R. Quhe, Y. Wang, Z. Ni, M. Ye, Z. Song, Y. Pan, J. Yang, L. Yang, M. Lei, J. Shi, J. Lu, Interfacial properties of monolayer and bilayer MoS₂ contacts with metals: beyond the energy band calculations. *Scientific Reports* **6**, 21786 (2016).
27. M. Matsunaga, A. Higuchi, G. He, T. Yamada, P. Kruger, Y. Ochiai, Y. Gong, R. Vajtai, P. M. Ajayan, J. P. Bird, N. Aoki, Nanoscale-barrier formation induced by low-dose electron-beam exposure in ultrathin MoS₂ transistors. *ACS Nano* **10**, 9730-9737 (2016).
28. J. R. Rumble, *CRC Handbook of Chemistry and Physics*. (CRC Press, ed. 89, 2000).
29. R. F. Bunshah, *Handbook of deposition technologies for films and coatings: science, technology, and applications*. (Elsevier Science & Technology Books, ed. 2, 1994).
30. American Welding Society, *Brazing Manual*. (American Welding Society, ed. 3, 1976).
31. H.-P. Komsa, J. Kotakoski, S. Kurasch, O. Lehtinen, U. Kaiser, A. V. Krasheninnikov, Two-Dimensional transition metal dichalcogenides under electron irradiation: defect production and doping. *Physical Review Letters* **109**, 035503 (2012).
32. W. Liu, J. Kang, W. Cao, D. Sarkar, Y. Khatami, D. Jena, K. Banerjee, High-performance few-layer MoS₂ field-effect-transistors with record low contact-resistance, in *2013 IEEE International Electron Devices Meeting*. 19.14.11-19.14.14 (2013).
33. C. U. Kshirsagar, W. Xu, Y. Su, M. C. Robbins, C. H. Kim, S. J. Koester, Dynamic memory cells using MoS₂ field-effect transistors demonstrating femtoampere leakage currents. *ACS Nano* **10**, 8457-8464 (2016).
34. K. D. Dorfman, P. Daoutidis, *Numerical Methods with Chemical Engineering Applications*. (Cambridge University Press, 2017).
35. E. J. Kirkland, *Advanced Computing in Electron Microscopy*. (Springer, New York, ed. 2, 2010).
36. R. J. Wu, A. Mittal, M. L. Odlyzko, K. A. Mkhoyan, Simplifying electron beam channeling in scanning transmission electron microscopy (STEM). *Microscopy and Microanalysis* **23**, 794-808 (2017).
37. J. L. Feldman, L. L. Boyer, Atomic mean-square displacements for 2H-MoS₂. *Solid State Communications* **37**, 879-881 (1981).
38. A. Mittal, D. B. Zhang, C. Teresi, T. Dumitrica, K. A. Mkhoyan, Routes to identification of intrinsic twist in helical MoS₂ nanotubes by electron diffraction and annular dark-field scanning transmission electron microscopy imaging. *Physical Review B* **84**, 153401 (2011).
39. P. A. Young, Lattice parameter measurements on molybdenum disulphide. *Journal of Physics D: Applied Physics* **1**, 936 (1968).
40. G. Kresse, J. Hafner, Ab initio molecular dynamics for liquid metals. *Physical Review B* **47**, 558-561 (1993).
41. G. Kresse, J. Hafner, Ab initio molecular-dynamics simulation of the liquid-metal–amorphous-semiconductor transition in germanium. *Physical Review B* **49**, 14251-14269 (1994).

42. G. Kresse, J. Furthmüller, Efficiency of ab-initio total energy calculations for metals and semiconductors using a plane-wave basis set. *Computational Materials Science* **6**, 15-50 (1996).
43. G. Kresse, J. Furthmüller, Efficient iterative schemes for ab initio total-energy calculations using a plane-wave basis set. *Physical Review B* **54**, 11169-11186 (1996).
44. J. P. Perdew, K. Burke, M. Ernzerhof, Generalized gradient approximation made simple. *Physical Review Letters* **77**, 3865-3868 (1996).
45. G. Kresse, D. Joubert, From ultrasoft pseudopotentials to the projector augmented-wave method. *Physical Review B* **59**, 1758-1775 (1999).
46. P. Blöchl, O. Jepsen, O. Andersen, Improved tetrahedron method for Brillouin-zone integrations. *Physical Review B* **49**, 16223-16233 (1994).
47. P. Schlexer, G. Pacchioni, Anchoring small Au clusters on the dehydroxylated and hydroxylated SiO₂ α -quartz (001) surface via Ti-alloying. *The Journal of Physical Chemistry C* **121**, 14717-14724 (2017).
48. A. R. Puigdollers, P. Schlexer, G. Pacchioni, Gold and silver clusters on TiO₂ and ZrO₂ (101) surfaces: role of dispersion forces. *The Journal of Physical Chemistry C* **119**, 15381-15389 (2015).
49. S. Grimme, Semiempirical GGA-type density functional constructed with a long-range dispersion correction. *Journal of Computational Chemistry* **27**, 1787-1799 (2006).
50. E. G. Moroni, G. Kresse, J. Hafner, J. Furthmüller, Ultrasoft pseudopotentials applied to magnetic Fe, Co, and Ni: from atoms to solids. *Physical Review B* **56**, 15629-15646 (1997).
51. J. A. Wilson, A. D. Yoffe, The transition metal dichalcogenides discussion and interpretation of the observed optical, electrical and structural properties. *Advances In Physics* **18**, 193-335 (1969).
52. Gatan, EELS atlas, <http://www.eels.info/atlas/titanium> (accessed: 2018)
53. Y. Wang, B. Wang, R. Huang, B. Gao, F. Kong, Q. Zhang, First-principles study of transition-metal atoms adsorption on MoS₂ monolayer. *Physica E: Low-dimensional Systems and Nanostructures* **63**, 276-282 (2014).
54. P. Wu, N. Yin, P. Li, W. Cheng, M. Huang, The adsorption and diffusion behavior of noble metal adatoms (Pd, Pt, Cu, Ag and Au) on a MoS₂ monolayer: a first-principles study. *Physical Chemistry Chemical Physics* **19**, 20713-20722 (2017).

Supplementary Materials:

Materials and Methods

Figures S1-S8

Tables S1-S17

Discussion on extension to other metals

References (29-54)

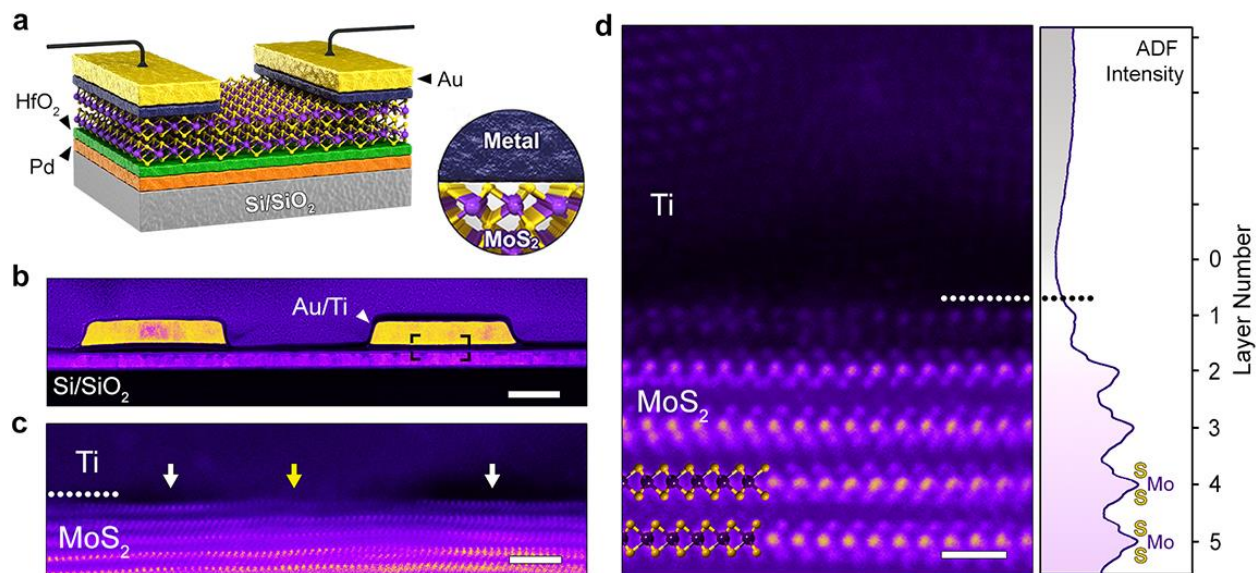


Fig. 1: Schematic layout and ADF-STEM images of a FET with MoS₂ channel: **a**, schematic layout of the FET showing the MoS₂ channel in contact with Au/Ti metal contacts and the remainder of the device. **b**, low-magnification cross-sectional ADF-STEM image of an actual FET prepared by FIB cutting. The protective amorphous C/Pt layers, also visible here, were deposited on top of the device during TEM sample preparation and are not part of the original FET. Scale bar is 0.2 μm . **c**, high-magnification image of the Ti-MoS₂ interface acquired from the boxed area in (b). An area where Ti is clustered is indicated by a yellow arrow, and areas with void pockets are indicated by white arrows. Slight distortions in the lower MoS₂ layers are due to small wrinkling of the MoS₂. Scale bar is 2 nm. **d**, atomic-resolution ADF-STEM image of the Ti-MoS₂ interface acquired from a Ti clustered area. The topmost layer of MoS₂ is visibly altered compared to the pristine-like layers below. The horizontally-averaged ADF intensity of the image is shown on the right. A ball-and-stick model of MoS₂ is overlaid on the image for clarity of atomic positions. Scale bar is 1 nm.

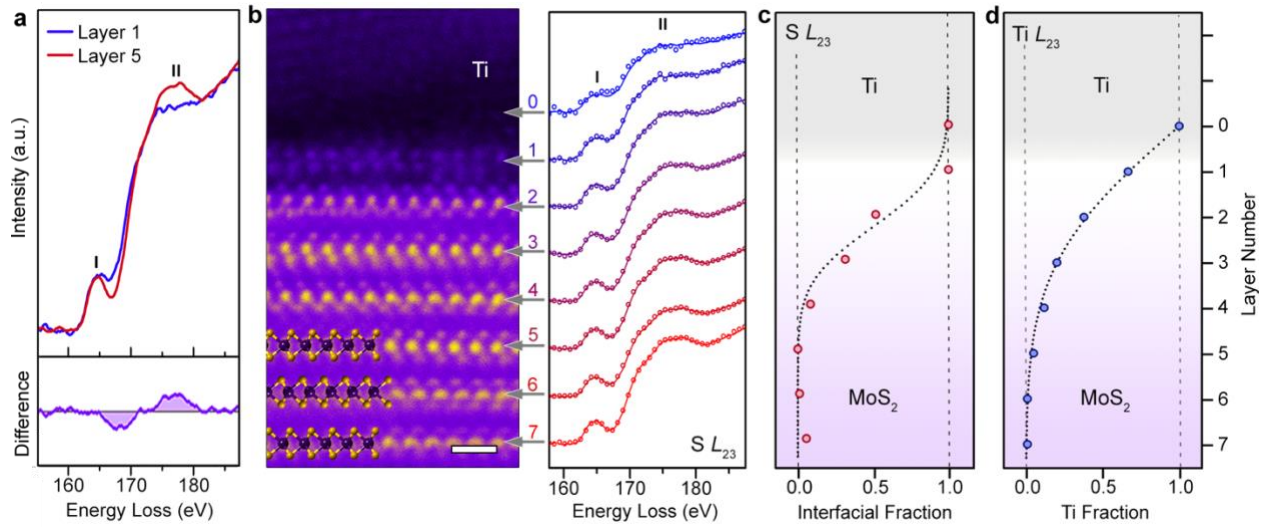


Fig. 2: Layer-by-layer core-level EELS across the Ti-MoS₂ interface: **a**, core-level EELS S L₂₃-edges measured from the first (nearest to Ti) and the fifth MoS₂ layers directly below the Ti contact. The differences between the two spectra are shown below. **b**, (left) atomic-resolution ADF-STEM image of the MoS₂ layers and (right) EELS S L_{2,3} edge measured at the corresponding layers shown in the left panel. A ball-and-stick model of MoS₂ layers is overlaid on the image for clarity. Scale bar is 1 nm. Measured spectra are shown as scatter points and fitted spectra are shown as lines. **c**, the fractions of the interfacial (reference layer 1) character in their S L₂₃ edge in each spectrum obtained from a linear superposition fit of the two reference spectra shown in (a). **d**, the fraction of Ti in MoS₂ layers evaluated by integrating the intensity of the measured EELS Ti L₂₃-edge obtained at each layer and normalized using the reference spectrum recorded from layer 0. A standard $y = \text{erf}(x)$ fit through the data points is shown for (c) and (d).

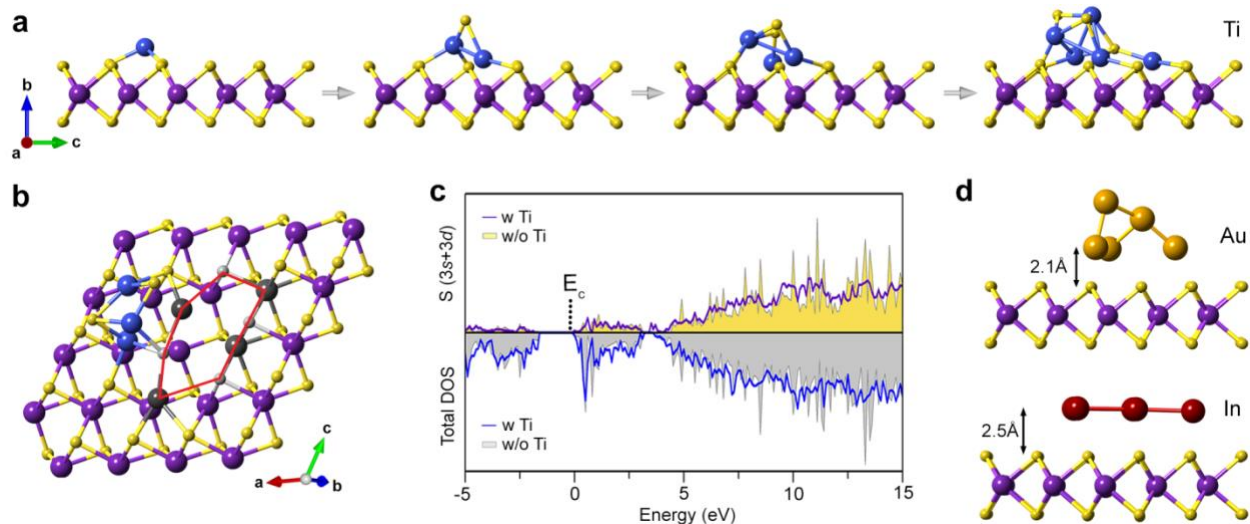


Fig. 3: Effects of small cluster of metals on atomic and electronic structure of MoS₂: **a**, ball-and-stick models showing the atomic positions for the lowest energy optimized structures of the Ti-MoS₂ system following additions of single Ti atoms up to five Ti atoms as determined by DFT calculations. **b**, a different perspective of Ti-MoS₂ system with 5 Ti atoms showing the distortions to the MoS₂ lattice. An opening in the lattice is outlined by the grey colored atoms and red line. **c**, the total and S 3s + 3d partial electronic DOS of pristine and five Ti atom-distorted MoS₂. Sulfur 3s and 3d partial-DOS are the states probed by EELS when measuring S L₂₃ edge. The bottom of the conduction band is used as the energy reference point in all cases. **d**, models showing the atomic positions for the lowest energy optimized structures of an Au-MoS₂ (top) and In-MoS₂ (bottom) system as determined by DFT calculations, similar to (a). In each case, 5 metal atoms and a monolayer of MoS₂ were used. The resulting distances between the sulfur atoms of MoS₂ and the closest metal atoms of the five-atom clusters are also indicated.